Impact of the atmospheric sink and vertical mixing on nitrous oxide fluxes estimated using inversion methods

R. Thompson, Philippe Bousquet, F. Chevallier, P. Rayner, Philippe Ciais

Impact of the atmospheric sink and vertical mixing on nitrous oxide fluxes estimated using inversion methods

R. L. Thompson,[1] P. Bousquet,[1] F. Chevallier,[1] P. J. Rayner,[1,2] and P. Ciais[1]

Received 14 February 2011; revised 13 June 2011; accepted 15 June 2011; published 14 September 2011.

[1] This study investigates some of the principal errors arising in atmospheric inversion estimates of N_2O surface fluxes. Using a synthetic data set of model-generated atmospheric N_2O mixing ratio data, representative of the current observation network, we investigate the influence of errors in the stratospheric N_2O sink and in vertical transport. Our inversion framework uses a variational formulation of the Bayesian problem, and atmospheric transport is modeled using the global circulation model LMDz. When only optimizing the surface fluxes (with a prescribed sink), bias errors in the sink magnitude translate into substantial bias errors in the retrieved global total surface fluxes. Conversely, we find that errors only in the temporal and horizontal distribution of the N_2O sink (nonbiased magnitude) have a very small impact on tropospheric mixing ratios and thus on the retrieved surface fluxes. Bias errors in the modeled vertical transport, however, lead to notable changes in tropospheric N_2O and, in particular, in the phase of the seasonal cycle. This also leads to bias errors in the spatial distribution of the derived surface fluxes, although not in the global total. Last, the simultaneous optimization of the surface fluxes and the sink magnitude was tested as a means to avoid biasing the fluxes by incorrect prior assumptions about the N_2O lifetime. With this approach, a significant reduction in the error of the sink magnitude was achieved and biases in the surface fluxes were largely avoided, and this result was further enhanced when aircraft data were included in the inversion.

Citation: Thompson, R. L., P. Bousquet, F. Chevallier, P. J. Rayner, and P. Ciais (2011), Impact of the atmospheric sink and vertical mixing on nitrous oxide fluxes estimated using inversion methods, *J. Geophys. Res.*, *116*, D17307, doi:10.1029/2011JD015815.

1. Introduction

[2] Nitrous oxide (N_2O) is a trace gas of significant interest to atmospheric sciences. Atmospheric levels of N_2O have been increasing steadily over the past few decades at a rate of approximately 0.3% per year [*Forster et al.*, 2007]. This trend is of major concern as N_2O is both a Greenhouse Gas (GHG) and the primary source of stratospheric NO and NO_2, which catalytically destroy ozone [*Crutzen*, 1970; *Johnston*, 1971]. Currently N_2O contributes an additional global radiative forcing of 0.16 Wm^{-2}, making it the fourth most important anthropogenic GHG after CO_2, CH_4 and CFC-12 [*Forster et al.*, 2007]. Since N_2O levels are very likely to continue increasing over the foreseeable future (in response to continued fertilizer production and use), while concentrations of CFC-12 are slowly declining, N_2O will soon overtake CFC-12 in its contribution to global warming. Recently the importance of N_2O as an ozone depleting substance (ODS) has also been recognized; emissions of N_2O are now thought to be the primary ODS emissions and of greater importance than those of CFCs [*Ravishankara et al.*, 2009], which have strongly declined as a result of the implementation of the Montreal Protocol on Substances that Deplete the Ozone Layer.

[3] The growth in atmospheric N_2O is predominantly due to the enhancement of N_2O emissions by human activities. Most notably, the intensification and proliferation of agriculture since the mid-19th century, which has been accompanied by the increased input of reactive nitrogen to soils, has resulted in significant perturbations to the natural N cycle and emissions of N_2O [*Galloway et al.*, 2008, and references therein]. Perturbations have also occurred in the marine N cycle due to the eutrophication of coastal waters [*Naqvi et al.*, 2000; *Nevison et al.*, 2004; *Seitzinger et al.*, 2000]. Emissions from other anthropogenic sources, such as industry (e.g., adipic and nitric acid production), municipal waste, and fossil fuel combustion, have also contributed to the observed trend in N_2O [*Olivier et al.*, 1998]. In total, human activities are thought to have increased the annual global N_2O emission by 40 to 50% over pre-industrial levels [*Denman et al.*, 2007]. Top-down studies estimate the contemporary emissions to be in the range of 16 to 17 TgN-N_2O/yr [*Corazza et al.*, 2010; *Hirsch et al.*, 2006; *Huang et al.*, 2008] while recent bottom-up estimates fall between 14 and 20.6 TgN-N_2O/yr [*Bouwman et al.*, 2002; *Denman et al.*, 2007] including nonbiogenic emissions. The accu-

[1] Laboratoire des Sciences du Climat et l'Environnement, Gif sur Yvette, France.
[2] Now at School of Earth Sciences, University of Melbourne, Melbourne, Victoria, Australia.

0148-0227/11/2011JD015815

mulation of N_2O in the atmosphere is attenuated by its removal from the atmosphere via photolysis and reaction with O^1D, which occur mostly in the stratosphere. The atmospheric lifetime of N_2O is thought, however, to have remained stable over the past century, as would be expected from a first-order-kinetics removal process, with a mean value of 122 ± 24 years [*Volk et al.*, 1997].

[4] Considering the importance of N_2O as a GHG and its role in ozone depletion, it is imperative to monitor, and if possible, eventually curb its emissions. Emission estimates can be ascertained globally and regionally by inversion of atmospheric N_2O mixing ratios with the aid of an atmospheric transport model. This 'inversion' approach has been previously employed in a number of global [*Corazza et al.*, 2010; *Hirsch et al.*, 2006; *Huang et al.*, 2008; *Prinn et al.*, 1990] and regional [*Manning et al.*, 2003; *Ryall et al.*, 2001; *Thompson et al.*, 2010] studies. The global studies differ significantly in the choice of statistical error model, atmospheric transport, as well as in their temporal and spatial resolution; however, there are some important sources of uncertainty common to all of them. First, all global inversions require an estimate of the atmospheric sink of N_2O in order to optimize the surface fluxes. Hitherto, this estimate has been prescribed in the setup and not optimized in the inversion (one exception to this is the early study of *Prinn et al.* [1990] in which the sink was optimized in conjunction with the surface fluxes using a simple global 9-box model of the atmosphere). Due to this dependency, one needs to have a handle on the sink magnitude in order to compare bottom-up with top-down estimates. The sink magnitude, derived from the total N_2O atmospheric abundance and its estimated lifetime, is approximately 12.5 TgN-N_2O/yr [*Denman et al.*, 2007] and carries an uncertainty of ±2.5 TgN-N_2O/yr (based on the given uncertainty of the atmospheric lifetime [*Volk et al.*, 1997]), which is equivalent to ±15% of the estimated global annual emission. The contribution of this uncertainty to surface flux estimates is illustrated in a sensitivity test performed by *Hirsch et al.* [2006], which estimated global total fluxes of 20.4 and 15.2 TgN-N_2O/yr for lifetimes of 98 and 146 years, respectively. Second, the uncertainty in vertical mass fluxes, calculated by the atmospheric transport model, also contributes to uncertainties in emission estimates, as has previously been pointed out for the case of CO_2 [*Stephens et al.*, 2007]. The vertical mass flux modulates the vertical gradient in N_2O, the abruptness of the transition of mixing ratio across the tropopause, and the mixing ratio of N_2O in the stratosphere. The impact of these uncertainties on the derived N_2O emissions needs to be quantified. Regional inversion estimates, which do not directly account for N_2O losses but take boundary mixing ratios from observations or models, are not sensitive to the sink uncertainty, so long as the mixing ratios from the vertical and upper horizontal boundaries match the observed N_2O growth rate.

[5] The goal of this study is to address the impacts of uncertainties in the N_2O sink and vertical mass fluxes in a global 4D atmospheric inversion framework by first providing estimates of the impact that these uncertainties have on the retrieved emissions and second, and principally, by including the magnitude of the N_2O sink in the inversion as a parameter to be optimized. The methodology for the simultaneous optimization of surface fluxes and the atmospheric sink is presented and its efficacy is tested using a global synthetic data set comprised of surface fluxes and atmospheric mixing ratios. In these tests, the utility of aircraft measurements for constraining both the surface fluxes and the sink is also assessed. For this study, we use a Bayesian inversion framework with a variational formulation, which is able to handle large numbers of variables, allowing higher temporal and spatial resolutions and thereby reducing aggregation errors in the optimized surface fluxes [*Kaminski et al.*, 2001]. This framework has already been used in a number of global inversions for CO_2 [*Chevallier et al.*, 2005], CH_4 [*Pison et al.*, 2009], CO [*Fortems-Cheiney et al.*, 2009], and H_2 [*Yver et al.*, 2010] and has been adapted for N_2O inversion for this study.

2. Method

2.1. Inversion Framework

[6] Bayesian inversions are increasingly used to optimize surface fluxes using the constraint of atmospheric observations. In this study, the Bayesian inversion is achieved using the variational framework of *Chevallier et al.* [2005]. This framework finds the optimal fluxes $\mathbf{x_a}$ that fit both the observed mixing ratios $\mathbf{y}$ and the prior fluxes $\mathbf{x_b}$ with their respective uncertainties. This can be written as the cost function:

$$J(\mathbf{x}) = (\mathbf{x}-\mathbf{x_b})^{\mathrm{T}}\mathbf{B}^{-1}(\mathbf{x}-\mathbf{x_b}) + (\mathcal{H}(\mathbf{x})-\mathbf{y})^{\mathrm{T}}\mathbf{R}^{-1}(\mathcal{H}(\mathbf{x})-\mathbf{y}) \tag{1}$$

where the flux uncertainties are described by the error covariance matrix $\mathbf{B}$, the observation uncertainties are described by the error covariance matrix $\mathbf{R}$, and $\mathcal{H}$ is an operator for atmospheric transport and chemistry. In the variational approach, the minimum of $J(\mathbf{x})$ is found iteratively, in this case, using a descent algorithm based on the Lanczos version of conjugate gradient algorithm [*Lanczos*, 1950]. This algorithm requires several computations of the gradient of J with respect to $\mathbf{x}$ (where $\mathbf{H}$ is the linearized form of $\mathcal{H}$):

$$\nabla_{\mathbf{x}} J(\mathbf{x}) = \mathbf{B}^{-1}(\mathbf{x}-\mathbf{x_b}) + \mathbf{H}^{\mathrm{T}}\mathbf{R}^{-1}(\mathcal{H}(\mathbf{x})-\mathbf{y}) \tag{2}$$

For very large problems (in terms of the number of variables), however, it is neither possible to directly define $\mathbf{H}$ nor $\mathbf{H}^{\mathrm{T}}$ owing to numerical limitations. Therefore, the elements of $\mathbf{H}^{\mathrm{T}}$ are found implicitly via the adjoint model of the atmospheric transport and chemistry [*Chevallier et al.*, 2005; *Errico*, 1997].

[7] In the case of N_2O, the sink in the stratosphere needs to be accounted for. Losses of N_2O occur via photolysis (reaction (R1)) and reaction with O^1D (reactions (R2) and (R3)), accounting for 90% and 10% of the sink, respectively [*Minschwaner et al.*, 1993]. These reactions are included in the forward and adjoint models of the atmospheric transport:

(R1) $$N_2O + h\nu \rightarrow N_2 + O^1D \ (90\%)$$

(R2) $$N_2O + O^1D \rightarrow 2NO \ (6\%) \ k_1 = 6.7 \times 10^{-11} \ cm^{-3}s^{-1}$$

(R3) $$N_2O + O^1D \rightarrow N_2 + O_2 \ (4\%) \ k_2 = 4.4 \times 10^{-11} \ cm^{-3}s^{-1}$$

Since only the loss of N_2O (and not the products of the reactions) is of interest here, these 3 equations can be combined into a single statement to update the mixing ratio c of N_2O for photolysis and chemistry in every grid cell of the forward model over the model time step t:

$$c_{i+1} = c_i - \lambda s_i c_i t \tag{3}$$

where $s_i = (k_1 + k_2)[O^1D]_i + \sigma_i$ is the total sink term, σ is the reaction cross section for photolysis (or equivalently the actinic flux), and λ is a scalar for the magnitude of the total sink. The number density of O^1D and the reaction cross-section σ are defined for each grid cell and time step and are taken from prior simulations of the global circulation and atmospheric chemistry model LMDZ-INCA [*Hauglustaine et al.*, 2004] with the same transport fields as used in the inversion. The tangent linear and adjoint statements for the N_2O mixing ratio c and for the sink scalar λ are derived from the following equation:

$$\frac{dc}{dt} = \frac{\partial c}{\partial t} - \lambda s \frac{\partial c}{\partial t} - sc \frac{\partial \lambda}{\partial t} \tag{4}$$

In this adaptation of the variational scheme, λ is included as a variable for optimization in the state vector $\mathbf{x}$ and has a prior value assigned in $\mathbf{x_b}$. One scalar λ is used to scale the sink term s for the vertical column in each of the latitudinal bands: 90°N–30°N, 30°N–0°, 0°–30°S, and 30°S–90°S, thus in total there are 4 sink scalars included in the state vector at each resolved time step. We refrained from using a higher resolution for the sink scalar optimization since very little is known about the spatial distribution of the errors of λ and how independent they would be.

[8] The flux and sink scalar variables in $\mathbf{x}$ are resolved in 4-weekly intervals. The choice of temporal resolution for the fluxes is a compromise between the time coverage of the available observations to constrain the fluxes, the number of state variables (which strongly determines the computational memory load) and the risk of temporal aggregation errors. Here the temporal resolution is consistent with that currently being used for global N_2O inversions [e.g., *Corazza et al.*, 2010]. Furthermore, the decision to temporally resolve the sink scalars (in this case at the same temporal resolution as the fluxes) was made to reduce the accumulation of rounding errors for each of the λ variables in the optimization algorithm, which would otherwise be considerable as each λ applies to all grid cells, horizontally and vertically, in its respective latitudinal band (i.e., for this model framework, in the order of 3×10^4 grid cells). Conversely, the spatial resolution of the fluxes was chosen to be at the highest possible horizontal resolution, that is, that of the transport model grid (3.75° × 2.5° longitude-latitude grid), in order to give the inversion scheme sufficient freedom to adjust small-scale flux patterns.

2.2. Atmospheric Transport Model

[9] The described inversion framework relies on an off-line version of the LMDz general circulation model [*Hourdin and Armengaud*, 1999; *Hourdin et al.*, 2006]. This version computes the evolution of atmospheric compounds, in this case N_2O, using archived fields of winds, convection mass fluxes, and planetary boundary layer (PBL) exchange coefficients that have been built from prior integrations of the complete general circulation model, which was nudged to ECMWF winds [*Uppala et al.*, 2005]. The LMDz model is on a 3D Eulerian grid consisting of 96 zonal columns and 73 meridional rows and 19 hybrid pressure levels in the vertical. The daytime PBL is resolved by 4–5 levels, the first of which corresponds to 70 m, and are spaced between 300 to 500 m apart from there upwards. Above the PBL the mean resolution is 2 km up to a height of 20 km, above which there are 4 levels with the uppermost level at 3 hPa. Tracer transport is calculated in LMDz using a second-order finite-volume method of *Van Leer* [1977] and is described for LMDz by *Hourdin and Armengaud* [1999]. Turbulent mixing in the PBL is parameterized using the scheme of *Mellor and Yamada* [1982] and thermal convection is parameterized according to the scheme of *Tiedtke* [1989]. LMDz was run with a physical time step of 30 min.

[10] For the calculation of the J and its gradient ∇J (equations (1) and (2)), the tangent linear $\mathbf{H}$ and adjoint $\mathbf{H}^T$ operators were coded from the off-line LMDz version [*Chevallier et al.*, 2005].

2.3. Synthetic Data

[11] Although the tests presented are performed using synthetic data, the data and their errors were chosen to best represent the magnitude and distribution of N_2O fluxes according to the current state of knowledge, and are commensurate with those used in the NitroEurope project [*Corazza et al.*, 2010]. Fields of monthly N_2O fluxes were compiled from anthropogenic (EDGAR-4.0), terrestrial biosphere (L. Bouwman, personal communication, 2008), and ocean [*Bouwman et al.*, 1995] fluxes. Anthropogenic emissions included those from agriculture, livestock, biomass burning, deforestation, agricultural waste burning, industry, and fossil and biofuel combustion. The fluxes were provided at 1° × 1° resolution and were interpolated to match the horizontal grid of the transport model. In total, the estimate of the global annual emission is 13.8 TgN-N_2O/yr, which is significantly lower than recent estimates of between 16 and 20 TgN-N_2O/yr [*Corazza et al.*, 2010; *Denman et al.*, 2007; *Hirsch et al.*, 2006; *Huang et al.*, 2008], therefore, the emissions were scaled up uniformly to give a global annual emission of 19 TgN-N_2O/yr, which resulted in an atmospheric growth rate close to that of the observed growth rate. These resulting fields are hereinafter referred to as the true fluxes as they were used in the generation of the synthetic observations (as described below).

[12] Since knowledge of the uncertainty of N_2O flux estimates is still limited, we calculated the uncertainty for each surface grid cell as 100% of the maximum flux for the year found in the 8 surrounding grid cells plus the cell of interest. This was done to allow more freedom in the inversion to correct the small-scale spatial pattern of the fluxes. (In some tests 50% of the maximum flux was used, as indicated in section 2.4). Correlations of surface flux errors were also incorporated into the definition of $\mathbf{B}$ and were calculated as an exponential decay with distance and time using correlation scale lengths of 500 km over land and 1000 km over ocean, and 8 weeks, respectively. The correlation scale length of the errors in land fluxes depends strongly on the source; here we chose 500 km as an educated guess to represent the correlation of the errors in the spatially diffuse soil emission, which

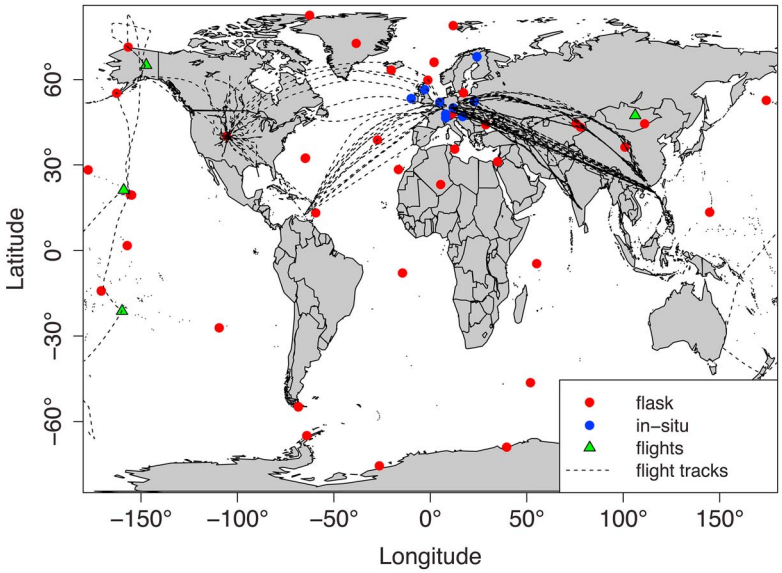

Figure 1. Map showing all sites where pseudo-observations were generated. In situ sites are in blue, flask-sampling sites are in red, and locations of regular aircraft measurements are in green. Flight paths for aircraft campaign measurements are shown by the black dashed lines.

is the dominant source and is modulated by land use, soil type, moisture and temperature, as well as by the amount of nitrogen input. For the inversions that include the optimization of the sink magnitude, **B** also contains error estimates for λ (of 50%, which equates to between 2.5 and 4 TgN-N_2O/yr). These were assumed to have no spatial correlation but a temporal correlation of 12 months.

[13] Pseudo-observations were generated for use in the inversion tests (i.e., S1 to S_{ref} and O1 to O3) and were consistent with a lifetime of 122 years [*Volk et al.*, 1997]. The pseudo-observations were produced for the years 2005 to 2008 by coupling the true fluxes (established above) to the forward LMDz model using the archived fields of winds, convection mass fluxes, and PBL exchange coefficients. The desired sink strength (and consequently the lifetime) was achieved by changing the value of λ, which scales the sink rate (one value of λ was used throughout the entire atmosphere and period of the simulation). The new λ for a lifetime τ is found from a reference lifetime τ_0, its corresponding λ_0, the atmospheric N_2O abundance A and the initial concentration c_i, according to equation (5) (derived from equation (3)) and was tested in forward model simulations.

$$\lambda = \lambda_0 \frac{\log\left(1 - \frac{A}{c_i \tau}\right)}{\log\left(1 - \frac{A}{c_i \tau_0}\right)} \tag{5}$$

For these LMDz simulations, starting mixing ratios were taken from a previous run of LMDz (of 8 years) that had reached quasi-steady state. In the generation of the mixing ratios, atmospheric loss of N_2O was calculated according to equation (3) using precalculated fields of σ and O^1D. Pseudo-observations were extracted from the 4-D fields of mixing ratios to best represent the actual current sampling network available (see Figure 1). We used the time stamps and locations of all the observations made available for use in the NitroEurope project [*Corazza et al.*, 2010] to extract the pseudo-observations from the synthetic data (see Table 1). For the continuous measurement sites at low elevation, only afternoon data were selected, while for mountain sites, only nighttime data were selected. In both cases, the selected data were assimilated hourly. In the real data, there are fewer surface observations in 2008; specifically only 2 of the European in situ sites had data in this year. Therefore, there are also fewer pseudo-observations for this year relative to 2006 and 2007. Additionally, we created pseudo aircraft observations using the flight tracks of the START and HIPPO campaigns (S. Wofsy, personal communication, 2010), as well as the CARIBIC passenger aircraft long range regular transects [*Brenninkmeijer et al.*, 2007] and NOAA (C. Sweeney, personal communication, 2010) routine flights, which were not included in the NitroEurope data set. The CARIBIC, START and HIPPO flight data include sampling locations up to 14 km, while the NOAA flight data extend up to 7 km. Of these data, approximately 35% were stratospheric samples while the remaining 65% were tropospheric samples. The pseudo aircraft data were subsampled so that only one data point was assimilated in the inversion per grid cell and time step of the model and where more than one observation was available, the mean was used. This was done in order to avoid assimilating highly correlated data, since correlations between observational errors were not accounted for (see below).

[14] Random Gaussian-distributed noise with a mean of 0 and SD of 0.2 ppb was added to the pseudo-observations to represent the errors in the measurements. These measurement errors were accounted for in the error covariance matrix **R**, which was defined as diagonal (there are no correlated errors in the observations). We chose to use an error of 0.2 ppb, instead of a larger error that would arguably be closer to the real value of the representation and measurement errors, so that the impact of bias errors in the

Table 1. Station Locations Where Pseudo-observations Were Generated[a]

Station	Coordinates		
ALT, Alert, Canada	82.5°N, 62.5°W, 200 m	KZM, Kazakhstan	43.3°N, 77.9°E, 2519 m
ASC, Ascension Isl.	7.9°S, 14.4°W, 54 m	MHD, Mace Head, Ireland	53.3°N, 9.9°W, 25 m
ASK, Assekrem, Algeria	23.2°N, 5.4°E, 2728 m	MID, Midway, USA	28.2°N, 177.4°W, 4 m
AZR, Terceira Isl., Azores	38.8°N, 27.4°W, 40 m	MLO, Mauna Loa, Hawaii	19.5°N, 155.6°W, 3397 m
BAL, Baltic Sea, Poland	55.4°N, 17.2°E, 3 m	NWR, Niwot Ridge, USA	40.1°N, 105.6°W, 3523 m
BIK, Bialystok, Poland	52.3°N, 22.8°E, 460 m	OXK, Ochsenkopf, Germany	50.1°N, 11.8°E, 1185 m
BME, Bermuda	32.4°N, 64.7°W, 30 m	PAL, Pallas, Finland	67.97°N, 24.1°E, 560 m
BMW, Bermuda	32.3°N, 64.9°W, 30 m	PFA, Poker Flat, Alaska, Flights	65.1°N, 147.3°W
BRW, Barrow, Alaska	71.3°N, 156.6°W, 11 m	PSA, Palmer Station, Antarctica	64.9°S, 64.0°W, 10 m
BSC, Black Sea, Romania	44.2°N 28.7°E, 3 m	RPB, Ragged Point, Barbados	13.2°N, 59.4°W, 45 m
CBW, Cabauw, Netherlands	52.0°N, 4.9°E, 198 m	RTA, Raratonga Flights	21.3°S, 159.8°W
CBA, Cold Bay, Alaska	55.2°N, 162.7°W, 21 m	SEY, Mahe Isl., Seychelles	4.7°S, 55.2°E, 3 m
CHR, Christmas Isl.	1.7°N, 157.2°W, 3 m	SHM, Shemya Isl., Alaska	52.7°N, 174.1°E, 40 m
CRZ, Crozet Isl.	46.5°S, 51.9°E, 120 m	SIL, Schauinsland, Germany	47.9°N, 7.9°E, 1205 m
EIC, Easter Isl.	27.2°S, 109.5°E, 50 m	SMO, Samoa	14.3°S, 170.6°W, 42 m
GMI, Mariana Isl.	13.4°N, 144.8°E, 1 m	SPO, South Pole	89.98°S, 24.8°W, 2810 m
HAA, Hawaii, Flights	21.2°N, 159.0°W	STM, Norway	66.0°N, 2.0°E, 0 m
HBA, Halley Station	75.6°S, 26.5°W, 30 m	SUM, Summit, Greenland	72.6°N, 38.5°W, 3238 m
HPB, Hohenpreißenberg Germany	47.8°N, 11.01°E, 985 m	SYO, Antarctica	69.0°S, 39.6°E, 11 m
HUN, Hegyhatsal, Hungary	47.0°N, 16.7°E, 248 m	TDF, Tierra del Fuego, Argentina	54.87°S, 68.5°W, 20 m
ICE, Iceland	63.4°N, 20.3°W, 118 m	TT1, Angus, Scotland	56.6°N, 3.0°W, 535 m
IZO, Tenerife, Canary Isl.	28.3°N, 16.5°W, 2360m	ULB, Ulaanbaatar Mongolia, Flights	47.4°N, 106.0°E
JFJ, Jungfraujoch, Switzerland	46.6°N, 8.0°E, 3580 m	UUM, Ulaan Uul, Mongolia	44.5°N, 111.1°E, 914 m
KUM, Kumukahi, Hawaii	19.5°N, 154.8°W, 3 m	WIS, Israel	31.1°N, 34.9°E, 400 m
KZD, Kazakhstan	44.1°N, 76.9°E, 601 m	WLG, Mt Waliguan, China	36.3°N, 100.9°E, 3810 m
LU1, Lutjewad, Netherlands	53.4°N, 6.4°E, 60 m	ZEP, Svalbard, Sweden	78.9°N, 11.9°E, 475 m

[a]Not including flight campaigns, i.e., CARIBIC and Harvard University flights.

transport and chemistry (photolysis and reaction with O^1D) model could be highlighted. The inversion tests (see section 2.4) isolate the impacts of these errors on the retrieved surface fluxes.

[15] Additionally, we used the forward LMDz model to perform a number of sensitivity tests for the impact of the sink strength and sink temporal and spatial distribution, as well as for vertical transport errors. The pseudo-observations, generated in these forward model runs, and the results from these tests are discussed in the supplementary material. Note that the pseudo data set P1, in the supplementary material, was also used as the observations in the following inversion tests.

2.4. Inversion Tests

[16] All inversion tests were performed for the years 2006 to 2008 and a summary of the tests is given in Table 2.

[17] Two inversion tests were designed to examine the impacts that incorrect assumptions in the spatial and temporal sink distribution and the vertical mass fluxes have on the retrieved N_2O surface fluxes (tests S1 and S2, respectively). In these two tests, the sink term is not optimized in the inversion, i.e., the sink scalar is static and the magnitude of the sink was equal to that used in the generation of the pseudo-observations (i.e., τ = 122 years). For both tests, the prior surface fluxes were equal to those of the true fluxes but with a prior uncertainty of 100%, to allow freedom in the inversion to adjust the surface fluxes according to the model–pseudo-observation mismatch induced by errors in either the atmospheric sink or the transport model.

[18] In test S1, errors were created in the temporal and spatial distribution of the atmospheric sink by replacing the true fields of actinic flux σ and O^1D (used in the tangent linear and adjoint calculations) with fields that had no temporal or horizontal variation. In this study, we decided not to test the impact of changing the vertical distribution of the stratospheric sink, even though this would have a strong impact on the magnitude of N_2O lost, as its impact is strongly dependent on the vertical resolution of the transport model used. In test S2, the vertical mass fluxes were perturbed by recycling the convective and advective mass fluxes from March 2006 for other every month, while the realistic fields of σ and O^1D were used.

Table 2. Summary of Inversion Tests

Test[a]	Optimize Sink	Number of Iterations	τ_{prior}	Prior Surface Fluxes	Prior Flux Uncertainty	Flight Data	O1D and σ Fields	Vertical Mass Fluxes
S1	no	20	122	equal to true	100%	no	flat	realistic
S2	no	20	122	equal to true	100%	no	realistic	recycled
S_{ref}	no	30	98	Perturbed	50%	no	realistic	realistic
O1	yes	30	122	Perturbed	50%	no	realistic	realistic
O2	yes	30	98	Perturbed	50%	no	realistic	realistic
O3	yes	30	98	Perturbed	50%	yes	realistic	realistic

[a]S, static sink (i.e., the sink was not optimized in the inversion); O, optimized sink (i.e., both surface fluxes and sink are optimized).

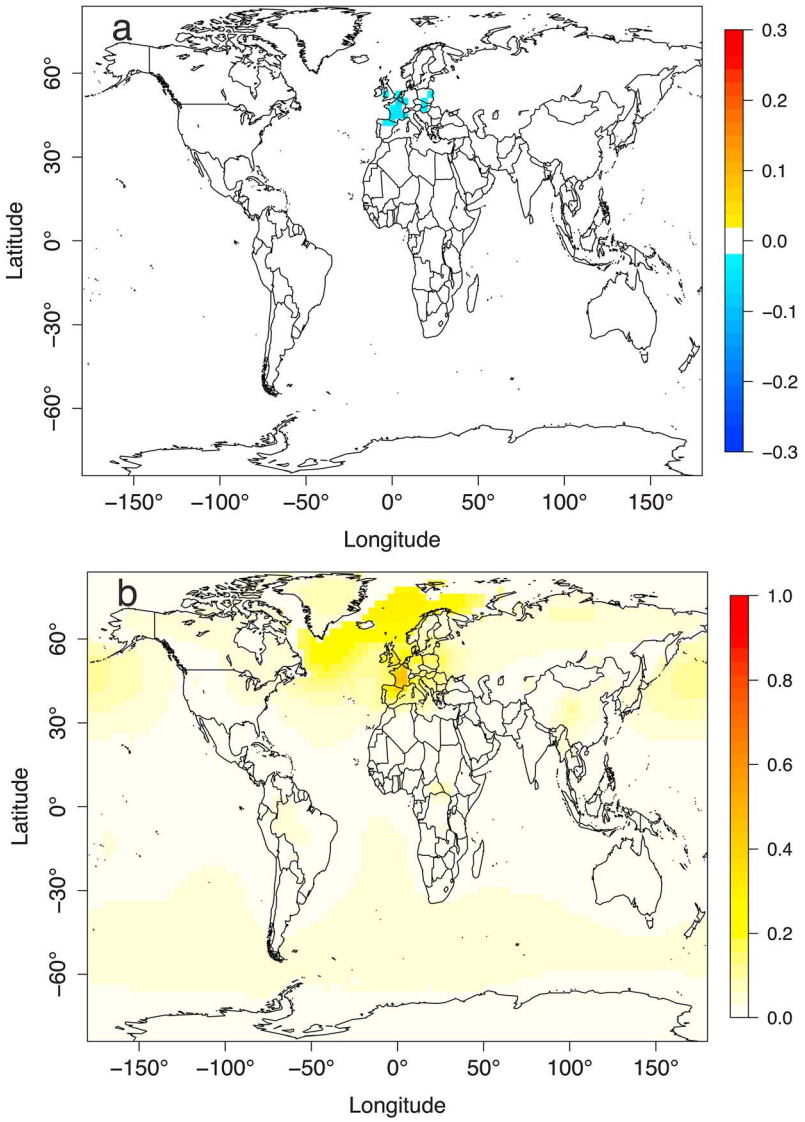

Figure 2. Inversion results for test S1, i.e., using sink terms that had no temporal or horizontal variability for calculation of N_2O loss in the model (a) annual mean difference in surface fluxes (posterior – prior) for 2007 in units of gN-N_2O/m^2/yr and (b) surface flux RMSE (posterior – true) for 2007, normalized by the mean prior surface flux.

[19] A reference inversion, S_{ref}, which also has a static sink (i.e., not optimized) was included to determine the impact of an incorrect assumption about the sink magnitude on the surface fluxes and forms a basis against which the following inversions, with sink optimization, can be assessed. The sink magnitude used in the transport and chemistry model was consistent with a lifetime of 98 years compared with the true value of 122 years used for the generation of the pseudo-observations. The prior surface fluxes in S_{ref} were formed by perturbing the true fluxes with random errors consistent with the errors in **B**, for which an uncertainty of 50% was used to be consistent with tests O1, O2 and O3 (see below).

[20] A set of 3 tests was designed to assess the efficacy of optimizing the sink term simultaneously with the surface fluxes. In accordance with test S_{ref}, these tests all start from the true surface fluxes that were perturbed with random errors and an uncertainty of 50%. The choice to use errors of 50% was made in order to limit the freedom for corrections to be made to the surface fluxes and thus allowing corrections to also be made to the sink scalars. The first test, O1, was made only to test how the inversion responds to the extra degrees of freedom provided by the inclusion of the sink scalars in the state vector for optimization; in this test the prior sink scalar was equal to the true sink scalar. The remaining 2 tests, O2 and O3, start from a biased prior sink scalar with a value of 1, which is consistent with a lifetime of 98 years, compared with the true value of 0.66 for which the lifetime is 122 years. O2 and O3 are identical with the

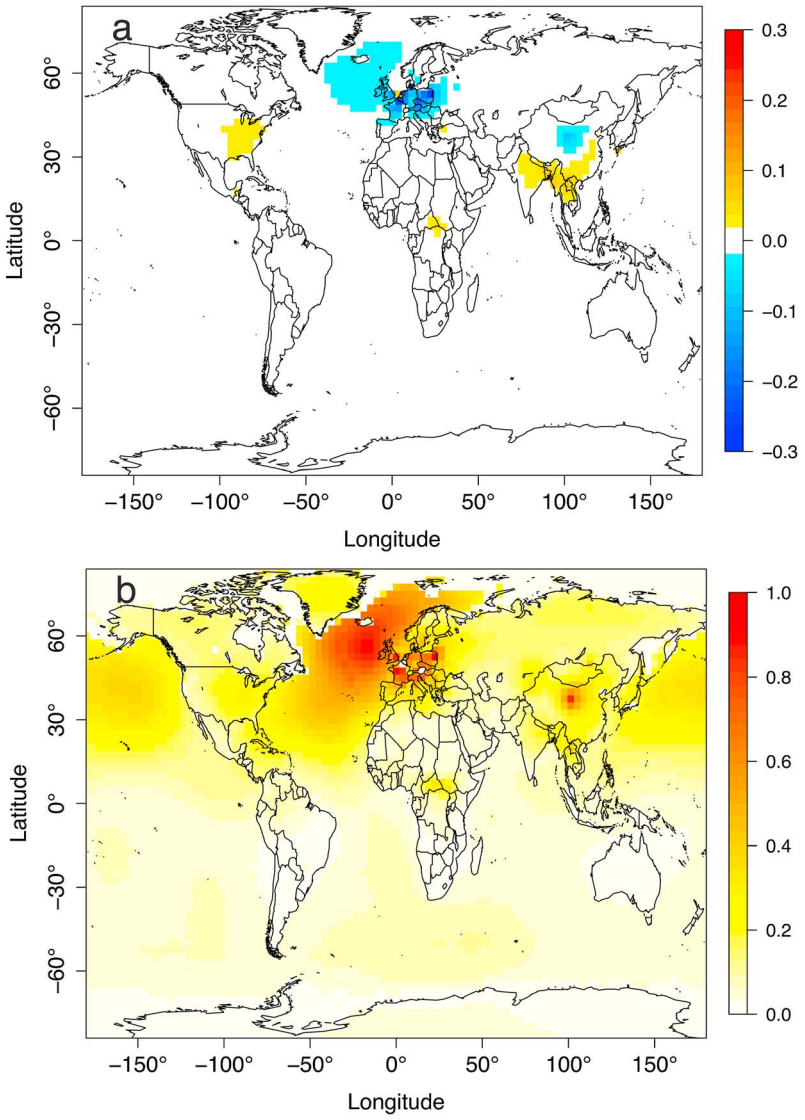

Figure 3. Inversion results for test S2, i.e., reusing the vertical mass flux for March 2006 for all months in the transport model (a) annual mean difference in surface fluxes (posterior – prior) for 2007 in units of $gN\text{-}N_2O/m^2/yr$ and (b) surface flux RMSE (posterior – true) for 2007, normalized by the mean prior surface flux.

exception that pseudo aircraft observations were included in O3 but not in O2.

3. Results and Discussion

3.1. Surface Flux Errors due to an Incorrect Sink Distribution

[21] The first of the tests with a static (i.e., not optimized) sink, S1, shows the impact that bias errors in the spatial and temporal distribution of the actinic flux σ and O^1D have on the retrieved surface fluxes. Test S1 most likely gives an overestimate for the error incurred in the fluxes, since the sink terms prescribed in S1 are far from being realistic (in that there is no difference between the winter and summer hemispheres). A forward simulation, using the same experimental setup (see test P3 in the auxiliary material), showed that changes in the distribution of the N_2O loss, and thus in the stratospheric N_2O mixing ratios, had little impact on the mixing ratios of N_2O in the troposphere, amounting only up to 0.1 ppb difference in the southern hemisphere.[1] Thus the mismatch between the (biased) forward-modeled and pseudo observed mixing ratios ($\mathcal{H}(\mathbf{x}) - \mathbf{y}$) is small. Consequently, the increments made to the surface fluxes are also small, and since the prior fluxes are equal to the true fluxes in this case (i.e., they have zero error), hence, there is also little bias error in the a posteriori surface fluxes (see Figure 2). The only regions where notable errors occur are Europe and the North Atlantic, which correspond to the region with the highest density of observations (in the case of the North Atlantic it is upwind of it). In Europe the annual

[1] Auxiliary materials are available in the HTML. doi:10.1029/2011JD015815.

mean error (posterior – true) is approximately 10% of the annual mean true surface flux. This region also coincides with large prior surface flux uncertainties, that is, where there is more freedom for flux adjustment. The mean surface flux increments are negative, reflecting the negative, albeit small, difference between the true and prior modeled tropospheric mixing ratios. For example, in 2007, the global total surface flux error was −0.57 TgN-N_2O (i.e., the posterior flux was less than the true flux), which is comparable to the expected value of −0.39 TgN-N_2O based on the model–pseudo-observation mismatch of approximately 0.1 ppb in the southern hemisphere (using a conversion factor of $7.75e^9$ kgN-N_2O/ppb).

3.2. Surface Flux Errors due to Incorrect Vertical Mixing

[22] The second test, S2, shows substantial errors in the a posteriori fluxes as a result of using incorrect vertical mass fluxes in the atmospheric transport model (see Figure 3). Again, these errors are most likely overestimates of the true error, because no seasonal variability in the vertical mass flux is accounted for in the recycled mass fluxes used in S2 and, additionally, no estimate of the transport uncertainty was included in the pseudo-observation prior error covariance matrix **R**. From Figure 3 it is apparent that the errors in the retrieved surface fluxes (induced by vertical transport errors) are predominant over the North Atlantic and Europe, where the magnitude is up to 25%, and over central China, south Asia, tropical Africa and the east coast of the USA where it is 5–10% of the prior surface flux. The positive increments over south Asia, tropical Africa and the east coast of the USA are the result of adjustments made to the surface fluxes in order to reduce the mismatch ($\mathcal{H}(\mathbf{x}) - \mathbf{y}$) in the troposphere caused by the underestimation of mixing ratios by the model using incorrect vertical mixing (refer to test P4 and Figures S4 and S5 in the auxiliary material). These regions also correspond with those where the prior surface flux uncertainties were high and fall upstream of measurement stations.

[23] In the model used in this test, the same prior surface fluxes and sink magnitude were used as that in the generation of the pseudo-observations, the only difference is that there has been a redistribution of N_2O in the vertical column owing to the change in vertical mass flux (although this has also indirect an impact on the horizontal N_2O distribution by changing the N_2O mixing ratio at altitudes where lateral transport occurs). The impact of changing the vertical transport is significant in the profiles of N_2O up to about 22 km; although the mixing ratios are generally lower in the troposphere they have actually increased throughout most of the year in the upper troposphere and lower stratosphere (see Figure S7). In order to maintain a global mass balance of N_2O, it is necessary to compensate the increase in surface fluxes, seen over south Asia, tropical Africa and the east coast of the USA, with an equivalent decrease. This decrease is allocated to Europe and the North Atlantic, which again are regions with high prior surface flux uncertainties. Here, the flux increments vary seasonally, with positive increments in February to March, coinciding with the period of the largest negative mismatch in ($\mathcal{H}(\mathbf{x}) - \mathbf{y}$), and with negative increments in July to September, when the mismatch is close to zero. For 2007, the difference in the global total surface flux (prior – posterior) was −0.05 TgN-N_2O.

3.3. Reference Inversion

[24] We performed a reference inversion (S_{ref}) using a biased sink (consistent with τ = 98 years compared with the true value of 122 years), which was not optimized in the inversion, to determine the magnitude of error incurred in the surface fluxes by this false assumption. Similar to the following inversion tests (in which the sink is optimized) the prior fluxes were perturbed with random errors according to **B**. This forms a reference against which the performance of the subsequent inversions (O1 to O3) can be assessed.

[25] Despite the biased sink, the random errors in the surface fluxes were significantly reduced as shown in the error reduction (ER) calculations where the ER is the ratio of the posterior over the prior root-mean-square error: $ER = 1 - RMSE_{post}/RMSE_{prior}$. Most of the error reduction (up to 50%) occurred over Europe, where there is the highest density of observations, and over the North Sea, a region that is still strongly constrained by the European observations (see Figure 4). In general, most of the reductions occurred in the proximity of stations, as expected. Although the random errors in the optimized surface fluxes were reduced, the bias (with respect to the true fluxes) increased over time, from close to zero in 2006 to 1.4 and 1.9 TgN-N_2O/yr in 2007 and 2008, respectively (see Table 3 and Figure 5). The influence of the sink magnitude bias on the N_2O growth rate only becomes apparent in 2007 (see Figure S1), owing to the time needed for this signal from the stratosphere to mix into the troposphere, explaining why the surface flux bias is close to zero for 2006, while in the following years the bias increases in order to counter the growing prior model–pseudo-observation mismatch. However, the increasing bias did not significantly influence the overall annual error reduction, as the RMS of the random errors is larger than that of the bias errors. Positive surface flux increments were made predominantly in 2007 over the high latitudes (north of 60°N) and south of South America (south of 60°S) and in 2008 over the North Atlantic, Siberia, and Alaska, while small negative increments were made in 2006 over Europe and the North Sea and in 2007 and 2008 over Europe and the Southern Ocean, consistent with the true–prior flux differences (see Figure 6a).

3.4. Simultaneous Optimization of Surface Fluxes and the Sink Magnitude

[26] The first of the tests for the simultaneous optimization of surface fluxes and sink magnitude, O1, starts from the randomly perturbed surface fluxes but with a sink magnitude equal to the true magnitude (i.e., equal to that which was used in the generation of the pseudo-observations). Both the sink magnitude and the surface fluxes were free to vary in the inversion within the prior errors defined in **B**. From the surface observations alone, there was sufficient information to produce significant reductions in the random surface flux errors resulting in a similar error reduction pattern to that in test S_{ref} (see Figure 4). Since there was no bias in the sink magnitude, the global total surface flux increments were in the correct direction to reduce the prior–true differences (see Figure 5). Although there was also freedom in the inversion to adjust the 4 sink scalars λ, in order to match the observed mixing ratios, only very small changes

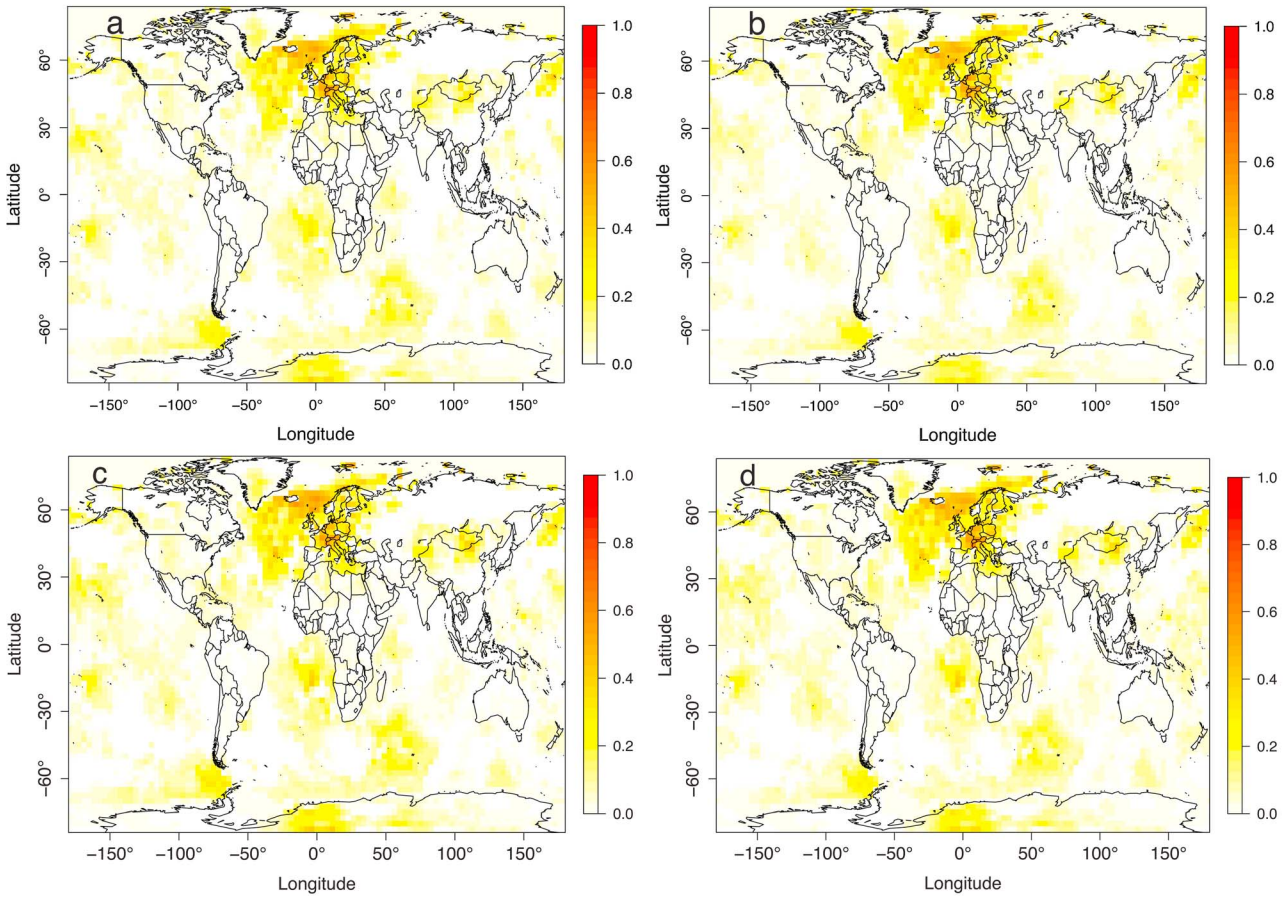

Figure 4. Error reduction in fluxes (1 – $RMSE_{post}/RMSE_{prior}$) shown for (a) test S_{ref} using no sink optimization and a prior sink magnitude consistent with (τ = 98 years), (b) test O1 using sink optimization but starting from the true sink magnitude (τ = 122 years), (c) test O2 using sink optimization and starting from a sink magnitude consistent with (τ = 98 years), and (d) test O3 using sink optimization (prior τ = 98 years) and including aircraft data.

in λ are observed (see Figure 6b) and amounted to only very small errors in the total sink magnitude (i.e., the differences between the sink magnitude used in the generation of the pseudo-observations and that calculated for the optimized model) of: 3.4%, 0.1% and 0.2% for 2006, 2007 and 2008, respectively (see Table 4).

[27] Test O1 shows that even if extra degrees of freedom are included, i.e., in the sink scalars, that the surface observations are still able to constrain the surface fluxes. Figure 7 shows that the posterior mixing ratios are in better agreement with the pseudo-observations (improved correlation and normalized SD) relative to the prior model owing to the corrections made to the surface fluxes through the inversion. However, in terms of the agreement with the

Table 3. Surface Flux Errors (prior/posterior – true) for the Tests S_{ref}, O1, O2 and O3 in TgN-N_2O/yr[a]

Year	Prior	S_{ref}	O1	O2	O3
2006	1.22	0.03	0.03	0.30	−0.16
2007	−1.04	1.35	0.01	0.51	−0.11
2008	−0.50	1.89	−0.67	0.64	−0.18

[a]Surface flux errors: prior/posterior – true.

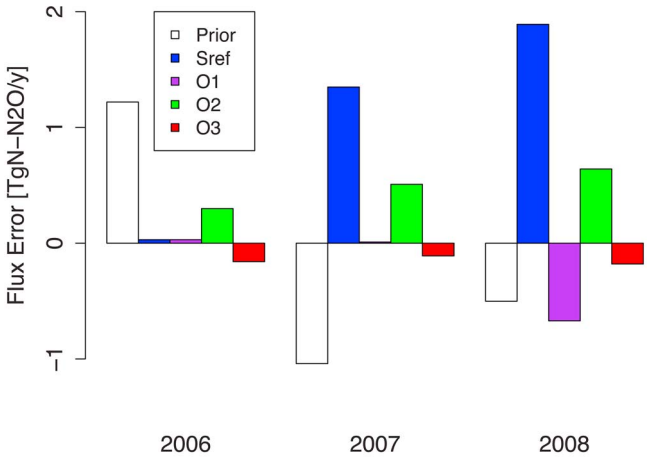

Figure 5. Comparison of flux errors from the prior model (white) and the inversion tests: S_{ref} using no sink optimization (blue), O1 using sink optimization but starting from the true sink magnitude (purple), O2 using sink optimization (green), and O3 using sink optimization and including aircraft data (red).

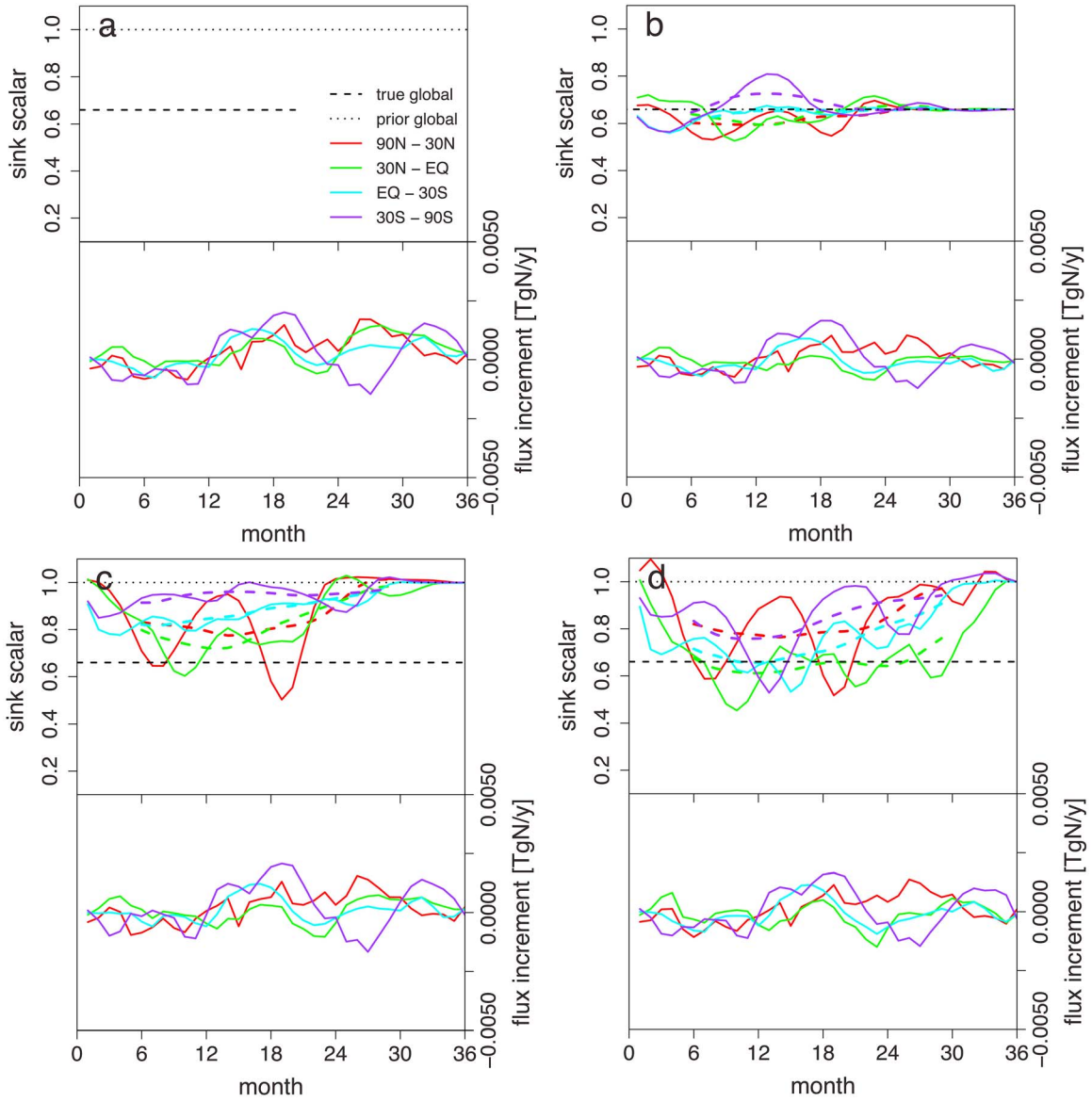

Figure 6. Sink scalars and integrated surface flux increments in each latitudinal band shown for (a) test S_{ref} using no sink optimization (prior τ = 98 years), (b) test O1 using sink optimization but starting from the true sink magnitude (prior τ = 122 years), (c) test O2 using sink optimization (prior τ = 98 years), and (d) test O3 using sink optimization (prior τ = 98 years) and including aircraft data. Also shown are prior (black dotted line) and true (black dashed line) sink scalar values and the 12 month running means of the optimized sink scalars (dashed lines) (note that for test O1 (Figure 6b) the prior sink was equal to the true value hence only one line is plotted (dash-dotted line)).

Table 4. Sink Magnitudes and Lifetimes and Surface Sources for the Tests S_{ref}, O1, O2, and O3 in TgN-N_2O/yr[a]

Year		True	Prior (S_{ref}, O2, O3)	Prior (O1)	Post (S_{ref})	Post (O1)	Post (O2)	Post (O3)
2006	Sink	11.8	14.6	11.8	16.0	11.4	13.7	12.2
		(125)	(100)	(125)	(93)	(130)	(108)	(121)
	Source	19.26	20.48	20.48	19.29	19.29	19.56	19.10
2007	Sink	12.3	15.0	12.3	15.3	12.3	14.2	12.8
		(120)	(97)	(120)	(97)	(121)	(105)	(116)
	Source	19.33	18.29	18.29	20.68	19.34	19.84	19.22
2008	Sink	12.3	14.8	12.3	14.9	12.3	15.3	15.1
		(120)	(98)	(120)	(100)	(121)	(97)	(99)
	Source	19.36	18.86	18.86	21.25	18.69	20.00	19.18

[a]The lifetimes (given in parentheses) were calculated using the actual abundances for each year and each scenario.

mixing ratios there is no significant difference between tests O1 and S_{ref}.

[28] In the second test, O2, the prior fluxes were perturbed, as was the case in O1, however, the prior sink scalar was equal to 1.0 (giving τ = 98 years) compared with the true value of 0.66 (τ = 122 years). Notable error reductions in the surface fluxes were observed and were comparable to those achieved in test O1 where the true sink magnitude was used (see Figure 4). Again, the largest error reductions occurred over the North Sea and central Europe, with other notable reductions in areas close to at least one measurement site. In this test, the error reduction was similar in all years.

[29] The ground-based observations range in altitude from 0 to 3810 m, corresponding to the sigma-pressure levels 1 to 7 (i.e., pressures 1004 to 663 hPa, when using a surface of 1013 hPa) in the transport model, thus, some comparison between the modeled and observed vertical gradient in N_2O is possible up to the free troposphere. These observations are also sensitive to the sink magnitude through its impact on the amplitude of seasonal cycle and the vertical gradient (see Figure S2). Adjustments to the sink scalars were predominantly made for the northern hemisphere, that is, to λ for the latitudinal bands 90 to 30°N and 30 to 0° (see Figure 6c) possibly due to the fact that all high altitude stations (>1000 masl) were in the northern hemisphere with the only exception being the South Pole (at 2810 masl).

[30] In contrast to the true and prior values of λ, which are constant in time, the posterior values show a strong seasonal dependence, with the northern hemisphere scalars reaching a minimum in summer while differing very little from the prior value in winter. Similarly, in the southern hemisphere, for the latitudinal band 30 to 90°S, the largest adjustment occurs in the austral summer. This result can be understood in terms of the mismatch between the prior and pseudo observed mixing ratios ($\mathcal{H}(\mathbf{x_b}) - \mathbf{y}$). In the northern hemisphere, the mixing ratios are underestimated by the prior at the time of the summer minimum, while the agreement is better for the winter maximum. To reduce this mismatch, an adjustment is made by the inversion to the summertime value of the sink scalar, rather than to the surface fluxes, because the summer minimum coincides with the period of strongest vertical mixing, when the entrainment of air from the stratosphere has a greater influence on the tropospheric mixing ratio. Conversely, in winter when the agreement is better and the vertical mixing is weaker, there is little adjustment made to the sink scalar value. The situation is similar in the southern hemisphere extratropics but with overall smaller changes; the minimum occurring in the austral summer also coincides with the period of strongest vertical mixing, thus the adjustment is made to the summertime sink scalar value. For the latitudinal band, 0° to 30°S, however, the amplitude of the seasonality is very small relative to the other latitudinal bands, most likely owing to the smaller amplitude of seasonal changes in vertical mixing.

[31] The reductions in the sink scalar errors were significant for 2006 and 2007, up to 59%, but were much smaller for 2008 (see Table 5). This has two causes: (1) it is partly due to the fact that there are fewer in situ observations in 2008 relative to the previous years and (2) that the observations, via the atmospheric transport function, represent the surface fluxes and the sink magnitude of up to several weeks and months into the past. This is particularly true for the sink, which is predominantly in the upper stratosphere, as its influence is only seen in the troposphere with a lag of up to several months depending on stratospheric mixing and the STE rate. Therefore, to well constrain the sink scalars in 2008, it would be necessary to include data from the first few months of 2009 (this is discussed further in relation to test O3).

[32] The oscillation in the posterior sink scalars, however, also represents a bias in the inversion, i.e., a summer-winter bias, which occurs despite using a 12 month correlation scale length. To overcome this bias, we calculated the 12 month running mean of the posterior values (see Figure 6) and recalculated the sink magnitudes for 2006 to 2007. In this case, the scalar means for each of the latitudinal bands (from north to south) are 0.83, 0.80, 0.82 and 0.91, and the corresponding lifetimes are 110, 112, 111 and 104 years, respectively, which are closer than the prior to the true value of 122 years.

[33] From Figure 7 it can be seen that the posterior mixing ratios compare very well with the pseudo-observations and that there is no loss in performance compared with tests S_{ref} and O1. The pseudo observed growth rate is also more closely matched by the posterior model owing to the seasonal reductions in the sink magnitude and the seasonal and shorter-term variations are better captured due to the corrections made to the surface fluxes (not shown). Moreover, compared with the posterior surface fluxes obtained in test S_{ref}, where the stratospheric sink had the same prior bias, the surface fluxes from test O2 were closer to the true fluxes and were not strongly biased (see Figure 5). For test O2, the errors in the total global surface flux (posterior – true) were 0.3, −0.5 and 0.6 TgN-N_2O/yr for 2006, 2007 and 2008, respectively (see Table 3).

[34] The third test, O3, was very similar to O2, with the exception that additional information was provided by the inclusion of pseudo aircraft data, again corresponding to

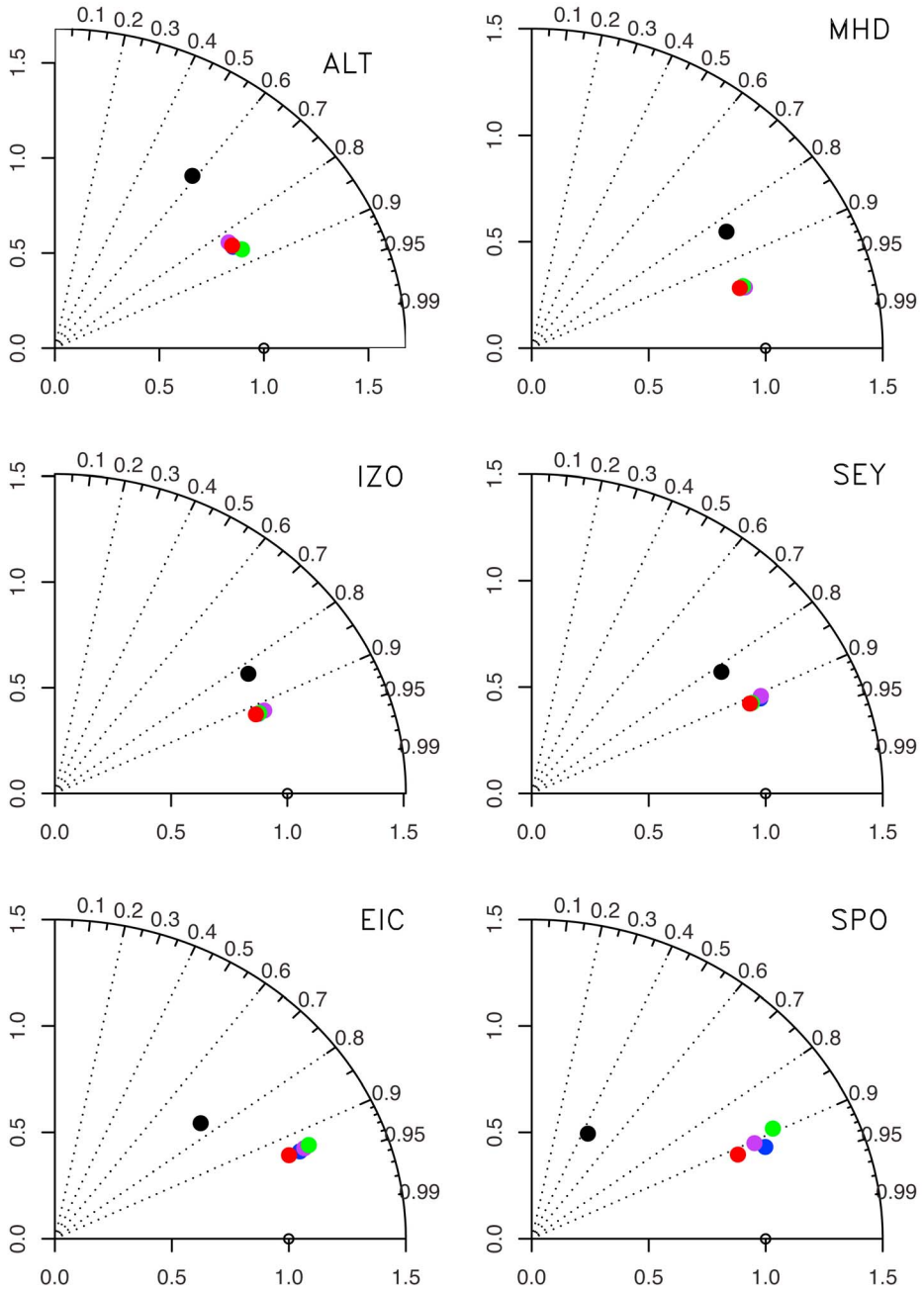

Figure 7. Taylor diagrams for the comparison of the observed N_2O mixing ratios and those simulated with different models at 6 representative sites (see Table 1 for site details). The radius indicates the normalized SD and the angle indicates the correlation coefficient. The data shown are the prior model (black dot), S_{ref} using no sink optimization (blue dot), O1 using sink optimization but starting from the true sink magnitude (purple dot), O2 using sink optimization but starting from the biased sink magnitude (green dot) and O3 using sink optimization starting from the biased sink but including in addition aircraft data (red dot).

the timestamps and locations of the real aircraft observations, which included observations at the altitudes of the tropopause and lower stratosphere (see section 2.3 for details). The inclusion of aircraft data did not result in any significant change in error reduction for the surface fluxes as compared with test O2 (see Figure 4). Nevertheless, it did result in greater reduction of the sink scalar errors; reductions of 85% and above were observed in the tropics and of 47% and above in the extratropics in 2006 and 2007 (see Table 5) and smaller bias errors in the fluxes. As discussed for test O2, the error reductions were much smaller for 2008, in particular for the sink scalars, owing to the fact that there were fewer in situ observations in 2008, and to the considerable time for mixing between the

Table 5. Error Reduction in Sink Scalars λ (Percent)

Latitudinal Band	O2			O3		
	2006	2007	2008	2006	2007	2008
90°E–30°N	50	59	0	53	63	6
30°N–0°	59	56	6	94	97	62
0°–30°S	53	32	9	85	87	21
30°–90°S	26	12	6	50	47	12

stratosphere and troposphere. However, by including the data from aircraft, some small reduction was still achieved for 2008 (more than in test O2) since the aircraft provide a more direct constraint on the sink. For the whole atmosphere, the posterior sink scalar values were equivalent to lifetimes of 121, 116 and 99 years for 2006, 2007 and 2008, respectively (see Table 4).

[35] Owing to the additional observational constraint provided by the pseudo aircraft data, the global total surface flux estimates were closer to those of the true fluxes than the posterior estimates obtained in tests S1 and O2 (see Figure 5). For O3, the errors in the total global surface flux were −0.2, −0.1 and −0.2 TgN-N_2O/yr for 2006, 2007 and 2008, respectively (see Table 3). The fact that test O3 performs better than O2 suggests that data from aircraft also provide, in addition to the constraint on the sink, a significant constraint on the surface fluxes. This hypothesis is consistent with a number of studies of airborne measurements that describe plumes with elevated concentrations of e.g., CO_2, CH_4 and N_2O in the free troposphere owing to rapid convective vertical transport of polluted boundary layer air. Observations inside and outside of the plume may be used to help constrain surface fluxes [*Machida et al.*, 2008; *Patra et al.*, 2011; *Schuck et al.*, 2010].

[36] The sink optimization tests presented have all been performed with pseudo-observations with no transport error. However, in reality, the optimization of the sink will be hampered by transport uncertainties. One error, in particular, is that of the Cross-Tropopause Flux (CTF), which is currently still largely unquantified. Since the CTF error (as well as other types of transport error) cannot be distinguished from that of the sink magnitude, the method we propose for the optimization of the sink will also partly compensate for these other errors in order to fit, for example, the vertical profile and the amplitude of the seasonal cycle. This effect is not necessarily undesirable, as it would avoid a bias in the surface fluxes (from both an incorrect sink magnitude and transport). However, ideally CTF error (and other transport errors) should be accounted for separately, in which case, the sink magnitude could be more accurately constrained.

4. Summary and Conclusions

[37] Using a synthetic data set, representative of the available atmospheric N_2O data globally, and a Bayesian inversion framework, the impacts of errors in vertical mixing and the stratospheric sink distribution on tropospheric N_2O mixing ratios and surface fluxes were investigated. Bias errors in the temporal and horizontal distribution of the sink terms (σ and O^1D) had very little impact on the tropospheric mixing ratios, whereas errors in the vertical mixing had a significant influence. The timing of the maximum in vertical mixing, with respect to the surface fluxes, was found to be important in determining the phase of the seasonal cycle, while overall changes in the strength of vertical mixing modulates the N_2O tropospheric growth rate before equilibrium is reestablished. The influence of errors in vertical mixing, however, was only significant up to about 22 km, above which the change in mixing ratio was relatively small and hence there was no impact on the sink magnitude. From the inversion tests, the retrieved surface fluxes were likewise found to be sensitive to vertical transport errors in the atmospheric model. Although, the global total surface flux was not biased, due to mass balance requirements, there were substantial errors in the spatial distribution. Conversely, the retrieved fluxes were not very sensitive to errors in the temporal and horizontal spatial distribution of the stratospheric sink via photolysis and the reaction with O^1D.

[38] The second, and main part of this paper, has examined the possibility of simultaneously optimizing the N_2O surface flux and the stratospheric sink. From the first tests presented here, there appears to be promise in this approach for reducing the bias errors that are introduced by incorrectly assuming the sink magnitude. The inversions carried out showed that there is sufficient information contained in the ground-based and aircraft observations to constrain the surface fluxes while simultaneously allowing the sink magnitude to be adjusted. In the cases where the prior sink magnitude was biased (i.e., assumed lifetimes of 98 years compared with the true lifetime of 122 years in tests O2 and O3), notable error reductions for the sink were achieved, while at the same time, the error reductions in the surface fluxes were similar to those found for the case with no bias in the prior sink (test O1), with reductions of up to 50%. Most importantly, by including the optimization of the sink, biases in the global total surface fluxes were substantially reduced, for example, for the inversion with a prior sink bias (τ = 98 years) but no sink optimization (test S_{ref}), a bias error of +1.9 TgN-N_2O/yr was obtained for 2008 compared with −0.2 TgN-N_2O/yr when the sink was also optimized (test O3).

[39] Since these tests were all performed using pseudo-observations and known atmospheric transport, the same reductions in the sink magnitude error are most likely not achievable with real observations, owing to the uncertainties in atmospheric transport. The method proposed for the optimization of the sink will also partly compensate for transport errors (as these cannot be clearly distinguished from the sink errors), with the same effect of reducing biases in the retrieved surface fluxes. Ideally, however, the transport errors would be accounted for separately, allowing for the sink magnitude to be constrained more accurately. In conclusion, it is important to consider the sink uncertainty in global inversions and to reduce the impact this has on the surface fluxes, especially in order to compare emissions estimates from this top-down approach with bottom-up estimates.

[40] **Acknowledgments.** We gratefully acknowledge the support of P. Bergamaschi and I. Pison for the work presented in this manuscript. R. Thompson was supported financially by the NitroEurope Project (SUS-TDEV-2004-3.I.1.1). P. Rayner is in receipt of an ARC Professorial Fellowship (DP1096309).

References

Bouwman, A. F., K. W. Van der Hoek, and J. G. J. Olivier (1995), Uncertainties in the global source distribution of nitrous oxide, *J. Geophys. Res.*, *100*(D2), 2785–2800, doi:10.1029/94JD02946.

Bouwman, A. F., L. J. M. Boumans, and N. H. Batjes (2002), Modeling global annual N_2O and NO emissions from fertilized fields, *Global Biogeochem. Cycles*, *16*(4), 1080, doi:10.1029/2001GB001812.

Brenninkmeijer, C. A. M., et al. (2007), Civil aircraft for the regular investigation of the atmosphere based on an instrumented container: The new CARIBIC system, *Atmos. Chem. Phys.*, *7*, 4953–4976, doi:10.5194/acp-7-4953-2007.

Chevallier, F., M. Fisher, P. Peylin, S. Serrar, P. Bousquet, F.-M. Bréon, A. Chédin, and P. Ciais (2005), Inferring CO_2 sources and sinks from satellite observations: Method and application to TOVS data, *J. Geophys. Res.*, *110*, D24309, doi:10.1029/2005JD006390.

Corazza, M., et al. (2010), Inverse modelling of European N_2O emissions: Assimilating observations from different networks, *Atmos. Chem. Phys. Discuss.*, *10*, 26,319–26,359, doi:10.5194/acpd-10-26319-2010.

Crutzen, P. J. (1970), The influence of nitrogen oxides on the atmospheric ozone content, *Q. J. R. Meteorol. Soc.*, *96*, 320–325, doi:10.1002/qj.49709640815.

Denman, K. L., et al. (2007), Couplings between changes in the climate system and biogeochemistry, in *Climate Change 2007: The Physical Science Basis. Contribution of Working Group I to the Fourth Assessment Report of the Intergovernmental Panel on Climate Change*, edited by S. D. Solomon et al., pp. 499–587, Cambridge Univ. Press, Cambridge, U. K.

Errico, R. M. (1997), What is an adjoint model?, *Bull. Am. Meteorol. Soc.*, *78*(11), 2577–2591, doi:10.1175/1520-0477(1997)078<2577:WIAAM>2.0.CO;2.

Forster, P., et al. (2007), Changes in atmospheric constituents and in radiative forcing, in *Climate Change 2007: The Physical Science Basis. Contribution of Working Group I to the Fourth Assessment Report of the Intergovernmental Panel on Climate Change*, edited by S. Solomon et al., pp. 129–234, Cambridge Univ. Press, Cambridge, U. K.

Fortems-Cheiney, A., F. Chevallier, I. Pison, P. Bousquet, C. Carouge, C. Clerbaux, P.-F. Coheur, M. George, D. Hurtmans, and S. Szopa (2009), On the capability of IASI measurements to inform about CO surface emissions, *Atmos. Chem. Phys.*, *9*, 8735–8743, doi:10.5194/acp-9-8735-2009.

Galloway, J. N., A. R. Townsend, J. W. Erisman, M. Bekunda, Z. Cai, J. R. Freney, L. A. Martinelli, S. P. Seitzinger, and M. A. Sutton (2008), Transformation of the nitrogen cycle: Recent trends, questions, and potential solutions, *Science*, *320*, 889–892, doi:10.1126/science.1136674.

Hauglustaine, D. A., F. Hourdin, L. Jourdain, M.-A. Filiberti, S. Walters, J.-F. Lamarque, and E. A. Holland (2004), Interactive chemistry in the Laboratoire de Météorologie Dynamique general circulation model: Description and background tropospheric chemistry evaluation, *J. Geophys. Res.*, *109*, D04314, doi:10.1029/2003JD003957.

Hirsch, A. I., A. M. Michalak, L. M. Bruhwiler, W. Peters, E. J. Dlugokencky, and P. P. Tans (2006), Inverse modeling estimates of the global nitrous oxide surface flux from 1998–2001, *Global Biogeochem. Cycles*, *20*, GB1008, doi:10.1029/2004GB002443.

Hourdin, F., and A. Armengaud (1999), The use of finite-volume methods for atmospheric advection of trace species. Part I: Test of various formulations in a general circulation model, *Mon. Weather Rev.*, *127*, 822–837, doi:10.1175/1520-0493(1999)127<0822:TUOFVM>2.0.CO;2.

Hourdin, F., et al. (2006), The LMDZ4 general circulation model: Climate performance and sensitivity to parameterized physics with emphasis on tropical convection, *Clim. Dyn.*, *27*, 787–813, doi:10.1007/s00382-006-0158-0.

Huang, J., et al. (2008), Estimation of regional emissions of nitrous oxide from 1997 to 2005 using multinetwork measurements, a chemical transport model, and an inverse method, *J. Geophys. Res.*, *113*, D17313, doi:10.1029/2007JD009381.

Johnston, H. (1971), Reduction of stratospheric ozone by nitrogen oxide catalysts from supersonic transport exhaust, *Science*, *173*, 517–522.

Kaminski, T., P. J. Rayner, M. Heimann, and I. G. Enting (2001), On aggregation errors in atmospheric transport inversions, *J. Geophys. Res.*, *106*(D5), 4703–4715, doi:10.1029/2000JD900581.

Lanczos, C. (1950), An iteration method for the solution of the eigenvalue problem, *J. Res. Natl. Bur. Stand. U. S.*, *45*, 255–282.

Machida, T., H. Matsueda, Y. Sawa, Y. Nakagawa, K. Hirotani, N. Kondo, K. Goto, T. Nakazawa, K. Ishikawa, and T. Ogawa (2008), Worldwide measurements of atmospheric CO_2 and other trace gas species using commercial airlines, *J. Atmos. Oceanic Technol.*, *25*, 1744–1754, doi:10.1175/2008JTECHA1082.1.

Manning, A. J., D. B. Ryall, and R. G. Derwent (2003), Estimating European emissions of ozone-depleting and greenhouse gases using observations and a modeling back-attribution technique, *J. Geophys. Res.*, *108*(D14), 4405, doi:10.1029/2002JD002312.

Mellor, G. L., and T. Yamada (1982), Development of a turbulence closure model for geophysical fluid problems, *Rev. Geophys.*, *20*(4), 851–875, doi:10.1029/RG020i004p00851.

Minschwaner, K., R. J. Salawitch, and M. B. McElroy (1993), Absorption of solar radiation by O_2: Implications for O_3 and lifetimes of N_2O, $CFCl_3$, and CF_2Cl_2, *J. Geophys. Res.*, *98*(D6), 10,543–10,561, doi:10.1029/93JD00223.

Naqvi, S. W. A., D. A. Jayakumar, P. V. Narvekar, H. Naik, V. V. S. S. Sarma, W. D'Souza, S. Joseph, and M. D. George (2000), Increased marine production of N_2O due to intensifying anoxia on the Indian continental shelf, *Nature*, *408*, 346–349.

Nevison, C. D., T. J. Lueker, and R. F. Weiss (2004), Quantifying the nitrous oxide source from coastal upwelling, *Global Biogeochem. Cycles*, *18*, GB1018, doi:10.1029/2003GB002110.

Olivier, J. G. J., A. F. Bouwman, K. W. Van der Hoek, and J. J. M. Berdowski (1998), Global air emission inventories for anthropogenic sources of NO_x, NH_3 and N_2O in 1990, *Environ. Pollut.*, *102*, 135–148, doi:10.1016/S0269-7491(98)80026-2.

Patra, P. K., Y. Niwa, T. J. Schuck, C. A. M. Brenninkmeijer, T. Machida, H. Hatsueda, and Y. Sawa (2011), Carbon balance of South Asia constrained by passenger aircraft CO_2 measurements, *Atmos. Chem. Phys. Discuss.*, *11*, 5379–5405, doi:10.5194/acpd-11-5379-2011.

Pison, I., P. Bousquet, F. Chevallier, S. Szopa, and D. Hauglustaine (2009), Multi-species inversion of CH_4, CO and H_2 emissions from surface measurements, *Atmos. Chem. Phys.*, *9*, 5281–5297, doi:10.5194/acp-9-5281-2009.

Prinn, R., D. Cunnold, R. Rasmussen, P. Simmonds, F. Alyea, A. Crawford, P. Fraser, and R. Rosen (1990), Atmospheric emissions and trends of nitrous oxide deduced from 10 years of ALE-GAGE data, *J. Geophys. Res.*, *95*(D11), 18,369–18,385, doi:10.1029/JD095iD11p18369.

Ravishankara, A. R., J. S. Daniel, and R. W. Portmann (2009), Nitrous oxide (N_2O): The dominant ozone-depleting substance emitted in the 21st century, *Science*, *326*, 123–125.

Ryall, D. B., R. G. Derwent, A. J. Manning, P. G. Simmonds, and S. O'Doherty (2001), Estimating source regions of European emissions of trace gases from observations at Mace Head, *Atmos. Environ.*, *35*, 2507–2523, doi:10.1016/S1352-2310(00)00433-7.

Schuck, T. J., C. A. M. Brenninkmeijer, A. K. Baker, F. Slemr, P. F. J. von Velthoven, and A. Zahn (2010), Greenhouse gas relationships in the Indian summer monsoon plume measured by the CARIBIC passenger aircraft, *Atmos. Chem. Phys.*, *10*, 3965–3984, doi:10.5194/acp-10-3965-2010.

Seitzinger, S. P., C. Kroeze, and R. V. Styles (2000), Global distribution of N_2O emissions from aquatic systems: Natural emissions and anthropogenic effects, *Chemosphere Global Change Sci.*, *2*, 267–279, doi:10.1016/S1465-9972(00)00015-5.

Stephens, B. B., et al. (2007), Weak northern and strong tropical land carbon uptake from vertical profiles of atmospheric CO_2, *Science*, *316*, 1732–1735, doi:10.1126/science.1137004.

Thompson, R. L., C. Gerbig, and C. Rödenbeck (2010), A Bayesian inversion estimate of N_2O emissions for western and central Europe and the assessment of aggregation errors, *Atmos. Chem. Phys. Discuss.*, *10*, 26,073–26,115, doi:10.5194/acpd-10-26073-2010.

Tiedtke, M. (1989), A comprehensive mass flux scheme for cumulus parameterization in large-scale models, *Mon. Weather Rev.*, *117*, 1779–1800, doi:10.1175/1520-0493(1989)117<1779:ACMFSF>2.0.CO;2.

Uppala, S. M., et al. (2005), The ERA-40 Reanalysis, *Q. J. R. Meteorol. Soc.*, *131*, 2961–3012, doi:10.1256/qj.04.176.

Van Leer, B. (1977), Towards the ultimate conservative difference scheme. Part IV: A new approach to numerical convection, *J. Comput. Phys.*, *23*, 276–299, doi:10.1016/0021-9991(77)90095-X.

Volk, C. M., J. W. Elkins, D. W. Fahey, G. S. Dutton, J. M. Gilligan, M. Loewenstein, J. R. Podolske, K. R. Chan, and M. R. Gunson (1997), Evaluation of source gas lifetimes from stratospheric observations, *J. Geophys. Res.*, *102*(D21), 25,543–25,564, doi:10.1029/97JD02215.

Yver, C., et al. (2010), A new estimation of the recent tropospheric molecular hydrogen budget using atmospheric observations and variational inversion, *Atmos. Chem. Phys. Discuss.*, *10*, 28,963–29,005, doi:10.5194/acpd-10-28963-2010.

P. Bousquet, F. Chevallier, P. Ciais, and R. L. Thompson, Laboratoire des Sciences du Climat et l'Environnement (LSCE), F- 91191 Gif sur Yvette, France. (rona.thompson@lsce.ipsl.fr)

P. J. Rayner, School of Earth Sciences, University of Melbourne, Melbourne, VIC 3010, Australia.